Gain-of-Function Mutations in *TRPM4* Cause Autosomal Dominant Isolated Cardiac Conduction Disease

Hui Liu, MS; Loubna El Zein, PhD; Martin Kruse, PhD; Romain Guinamard, PhD; Alf Beckmann, PhD; André Bozio, MD; Güven Kurtbay, MS; André Mégarbané, MD, PhD; Iris Ohmert, BS; Gérard Blaysat, MD; Elisabeth Villain, MD; Olaf Pongs, PhD; Patrice Bouvagnet, MD, PhD

Background—Isolated cardiac conduction block is a relatively common condition in young and elderly populations. Genetic predisposing factors have long been suspected because of numerous familial case reports. Deciphering genetic predisposing factors of conduction blocks may give a hint at stratifying conduction block carriers in a more efficient way.

Methods and Results—One Lebanese family and 2 French families with autosomal dominant isolated cardiac conduction blocks were used for linkage analysis. A maximum combined multipoint lod score of 10.5 was obtained on a genomic interval including more than 300 genes. After screening 12 genes of this interval for mutation, we found a heterozygous missense mutation of the *TRPM4* gene in each family (p.Arg164Trp, p.Ala432Thr, and p.Gly844Asp). This gene encodes the TRPM4 channel, a calcium-activated nonselective cation channel of the transient receptor potential melastatin (TRPM) ion channel family. All 3 mutations result in an increased current density. This gain of function is due to an elevated TRPM4 channel density at the cell surface secondary to impaired endocytosis and deregulation of Small Ubiquitin MOdifier conjugation (SUMOylation). Furthermore, we showed by immunohistochemistry that TRPM4 channel signal level is higher in atrial cardiomyocytes than in common ventricular cells, but is highest in Purkinje fibers. Small bundles of highly TRPM4-positive cells were found in the subendocardium and in rare intramural bundles.

Conclusions—the *TRPM4* gene is a causative gene in isolated cardiac conduction disease with mutations resulting in a gain of function and TRPM4 channel being highly expressed in cardiac Purkinje fibers. **(*Circ Cardiovasc Genet*. 2010;3:374-385.)**

Key Words: bundle-branch block ■ heart block ■ ion channel ■ sudden death ■ genetics

Downloaded from http://ahajournals.org by on February 7, 2019

Conduction block is a condition in which the depolarization wave initiated in the sinus node of the heart is slowed down or even blocked on the way to ventricular cardiomyocytes. The position of the block, its completeness (partial or complete), and the number of blocks are largely variable from one individual to the other. Conduction blocks are not rare in the general population either among young people or late in life. Right bundle-branch block (RBBB) has a prevalence of about 0.1% in normal children, with a male predominance.[1] Complete RBBB with normal left ejection fraction and no diagnoses of cardiac disease was observed in 0.3% of individuals in a population of adults with a median age of 64 years in a community-based study lead by Miller et al.[2] The natural evolution of isolated conduction blocks is unpredictable, and deciphering the genetic predisposing factors might help in unmasking those that are dangerous. Rare cases of familial conduction blocks are secondary to mutations in *SCN5A*[3] or *NKX2.5*.[4] In the latter gene, the conduction block is often associated with a congenital heart defect (typically an atrial septal defect). Recently, a South African family with cardiac conduction block was reported to carry a mutation in transient receptor potential melastatin (*TRPM4*).[5]

Editorial on p 311
Clinical Perspective on p 385

In the present study, we reported on 3 families with diverse conduction blocks transmitted with an autosomal dominant inheritance and incomplete penetrance. All 3 families were

Received December 11, 2009; accepted May 5, 2010.

From Université de Lyon (H.L., L.E.Z., P.B.), Laboratoire Cardiogénétique, Equipe d'Accueil 4171, Lyon, France; Hospices Civils de Lyon (H.L., L.E.Z., P.B.), Groupe Hospitalier Est, Laboratoire Cardiogénétique, Bron, France; Institut für Neurale Signalverarbeitung (M.K., A.B., G.K., I.O., O.P.), Zentrum für Molekulare Neurobiologie, Universität Hamburg, Hamburg, Germany; Université de Caen (R.G.), Laboratoire d'Anesthésiologie Expérimentale et Physiologie Cellulaire, Equipe d'Accueil 3212, Caen, France; Hospices Civils de Lyon (A.B., P.B.), Groupe Hospitalier Est, Service de Cardiologie Pédiatrique, Bron, France; Unité de Génétique Médicale (A.M.), Faculté de Médecine, Université Saint Joseph, Beirut, Lebanon; Unité de Recherche UMR_S 910, Service de Génétique Médicale, Faculté de Médecine de la Timone, Marseille, France; CHU Grenoble, Hôpital Michallon (G.B.), Service de Cardiologie Pédiatrique, Grenoble, France; and Service de Cardiologie (E.V.), Hôpital Necker-Enfants Malades, Paris, France.

Drs Liu, El Zein, and Kruse contributed equally to the work.

The online-only Data Supplement is available at http://circgenetics.ahajournals.org/cgi/content/full/CIRCGENETICS.109.930867/DC1.

Correspondence to Patrice Bouvagnet, MD, Laboratoire Cardiogénétique, CBPE, Groupe Hospitalier Est, 59 Boulevard Pinel, 69677 Bron, France. E-mail Patrice.Bouvagnet@chu-lyon.fr

© 2010 American Heart Association, Inc.

Circ Cardiovasc Genet **is available at http://circgenetics.ahajournals.org** **DOI: 10.1161/CIRCGENETICS.109.930867**

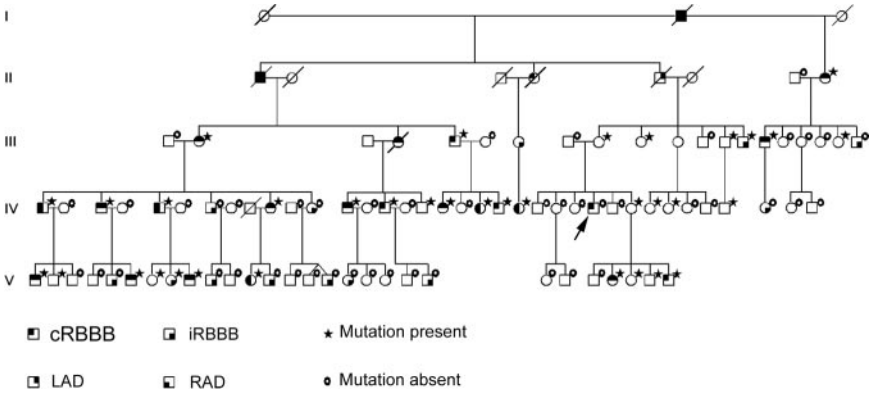

Figure 1. Partial pedigree of the Lebanese family (L1). The symbols of various cardiac conduction types and carrier status are explained at the bottom of the figure. Generation numbers are indicated to the left. Arabic numbers are assigned for each generation from left to right starting with 1. cRBBB indicates complete RBBB; and iRBBB, incomplete RBBB.

consistent with a mutation on the long arm of chromosome 19 in an interval containing about 300 genes. After screening for 12 genes, we found missense mutations in each family. These mutations did not modify the biophysical properties of TRPM4 but increased current density at the surface of transfected HEK293 cells. In addition, we showed that this increase in current density is probably secondary to endocytosis alteration and deregulation of Small Ubiquitin MOdifier conjugation (SUMOylation). Finally, with a TRPM4-specific antibody, we showed that Purkinje fibers expressed high levels of TRPM4 channel.

Materials and Methods

Clinical Evaluation

Medical and surgical histories of participants were recorded. A 12-lead ECG recording and a blood sample were obtained. Earlier cardiological examinations (ECG, echocardiogram, and others) were obtained when available. Individuals were considered affected if the ECG demonstrated a conduction disorder (complete RBBB with or without QRS frontal-axis deviation ($\leq$30 or $\geq$100°), incomplete RBBB with a QRS frontal-axis deviation, isolated QRS frontal-axis deviation, or RBBB and a first-degree atrioventricular block in the absence of other causes. Individuals with an incomplete RBBB (QRS width $<$120 ms) were considered normal.[6]

The study was approved by the local ethical committee. A signed informed consent was obtained from the participants (or the parents of minors) before history recording and blood drawing.

Genotyping and Linkage Analysis

DNA was extracted according to standard protocols. All individuals with DNA available were genotyped. They are indicated on Figures 1, 2A, and 2B with a star (carrier) or a circle (noncarrier). Altogether, 81 individuals were genotyped in family L1 (35 carriers, 46 noncarriers): 19 individuals in family F1 (12 carriers and 7 noncarriers) and 14 in family F2 (10 carriers, 4 noncarriers). Primers and map locations were based on Ensembl databases. PCR amplicons were analyzed on an ABI Prism 3130xl Genetic Analyzer (Foster City, Calif). Genemapper 4.0 sofware assigned the allele distribution (Applied Biosystems). Linkage analysis was carried out through easyLinkage Plus 5.08.[7] EasyLinkage was designed to make the use of linkage programs user-friendly and to enable those analyses on Microsoft Windows-based operating systems. Multipoint analysis was done with GeneHunter v2.1r5,[8] using a mutation prevalence and penetrances as described earlier[9] and a phenocopy rate of 0.1%. The polymorphic markers used were D19S606, D19S596, HRC, D19S879, D19S604, D19S866, D19S867, D19S904,

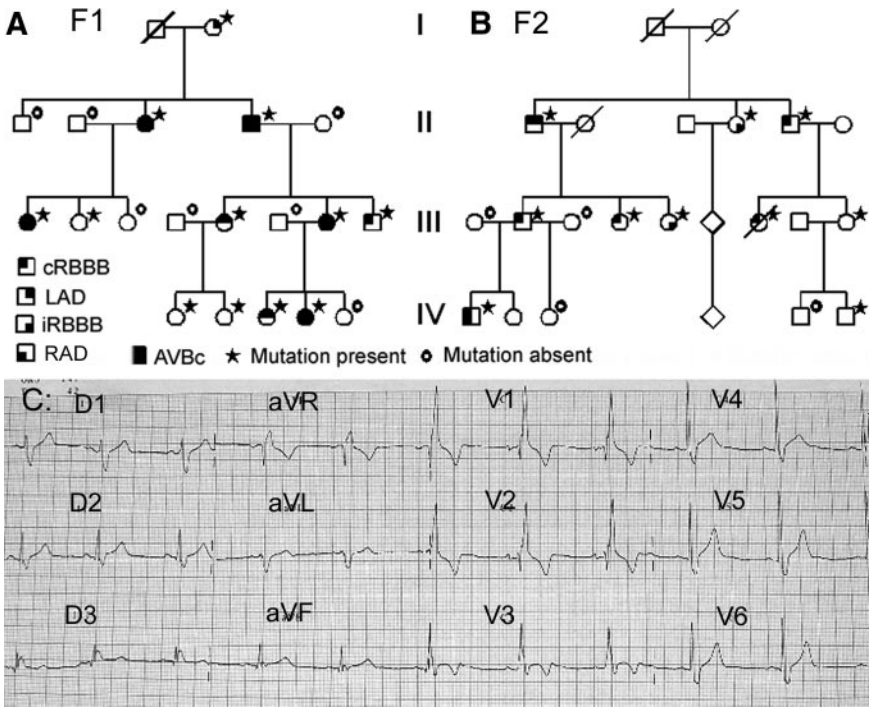

Figure 2. Pedigree of families F1 and F2 and an ECG with a bifascicular conduction block. A, Pedigree of French family F1 with the legend indicating the type of cardiac conduction block and the mutation status of family members. B, Pedigree of French family F2. C, ECG of patient IV.1 of family F2 showing a complete RBBB (cRBBB) with a right-axis deviation (RAD).

Downloaded from http://ahajournals.org by on February 7, 2019

D10S246, KLK1, D19S601, and D19S571 (from telomere to centromere, according to the LDB STRP map).

If individual IV-26 (arrow in Figure 1) is considered as affected instead of undetermined, the peak multipoint lod score of family L1 drops to 4.73 and 4.74, depending on the phenocopy rate (0.0% and 0.1%, respectively). Carriage return two-point linkage analysis between TRPM4 mutations and the disease phenotype gave lod scores of 8.79 (6.47, 1.54, and 0.78), with a phenocopy rate of 0.1% if individual IV-26 is considered as undetermined and 7.61 (5.29, 1.54, and 0.78) if this individual is considered as affected.

This individual was initially (individual IV-25 of Figure 1 in de Meeus et al, 1995[6]) considered as undetermined because he had an isolated incomplete RBBB. He presented with a complete RBBB by 1997 (Figures 5A and 6B in Stephan et al[9]) and was considered as a phenocopy because his complete RBBB was different from the other RBBB of family L1 and he was not carrying the mutation haplotype.

Sequencing

Mutational analysis of genes was carried out by bidirectional direct sequencing of amplified genomic DNA amplicons with intron-based, exon-specific primers (online-only Data Supplement Table). Control DNAs were analyzed by PCR, restriction enzyme digestion and agarose gel migration.

Cloning of Expression Plasmids

The cDNA of TRPM4 was obtained in 2 overlapping fragments from human kidney RNA (Stratagene, Amsterdam, The Netherlands) by reverse transcription with Mu-MLV Reverse transcriptase (Eurogentec France SASU, Angers, France). The complete TRPM4 cDNA was cloned in pcDNA4/TO vector (Invitrogen, Cergy Pontoise, France). Primers for reverse transcription and PCR are available on request.

The following cDNAs were cloned into pcDNA3-vector: human TRPM4 (provided by A. Guse, University Hospital Hamburg-Eppendorf),[10] dynamitin (provided by R. Vallee, Columbia University, New York),[11,12] SENP1 (provided by P. O'Hare, Marie Curie Research Institute, Oxted),[13] and Ubc9 (provided by S. Müller, Max-Planck-Institute of Biochemistry, Munich).[14] Mutant and tagged TRPM4-cDNAs were obtained by in vitro mutagenesis using the QuickChange II site-directed mutagenesis kit (Stratagene). Mutant cDNA clones were systematically resequenced before used in further experiments.

Cell Culture

Human embryonic kidney 293 (HEK-293), Chinese hamster ovary (CHO), and African green monkey (COS-7) cells were cultured at 37°C/5% CO_2 in Dulbecco modified Eagle medium (HEK-293 and COS-7) or Minimum Essential Medium–α-medium (CHO) supplemented with 10% fetal bovine serum (Invitrogen Inc) and 2 mmol/L glutamine. Plasmid DNA was transfected into HEK-293, COS-7, and CHO cells with Lipofectamine 2000 (Invitrogen Inc) according to manufacturer specifications.

Immunofluorescence

COS-7 cells were plated onto glass cover slips and transiently transfected with expression plasmids for wild-type and mutant TRPM4, respectively. Both plasmid types have a FLAG tag insertion after the first methionine. Forty-eight hours after transfection, cells were fixed with 4% paraformaldehyde and permeabilized with 0.2% Triton X-100. After blockade for unspecific binding with 10% horse serum, cells were stained for TRPM4-expression by mouse FLAG-specific antibody (Sigma Aldrich, Germany) at a dilution of 1:500 at 22°C for 1 hour. After washing, cells were treated with a goat anti-mouse secondary antibody coupled to Alexa Fluor 546 (Molecular Probes) for 20 minutes at 22°C at a dilution of 1:1000. Stained cells were analyzed with a Fluoview FV1000 confocal microscope (Olympus GmbH, Germany). For each genotype, digital pictures of 60 cells were chosen randomly and signal intensity over entire cells was quantified by using ImageJ software (http://rsbweb.nih.gov/if/). Mean fluorescence intensities, standard deviations, and SEM values for each genotype were calculated with Microsoft Excel software. To test for statistical significance between fluorescence intensities of different genotypes, the Student t test was used. probability values below 0.05 were considered significant.

Electrophysiology

Whole-cell, inside-out, and single-channel patch-clamp recordings were performed with an EPC9 patch-clamp amplifier (HEKA Elektronik, Germany) at a sampling rate of 20 kHz. Patch electrodes had a DC resistance between 1 and 3 mol/MΩ when filled with intracellular solution for whole-cell and inside-out patches and between 6 and 10 mol/MΩ for single-channel recordings. An Ag-AgCl wire was used as a reference electrode. Capacitance and access resistance were monitored continuously; cell membrane capacitance values were used to calculate current densities. For whole-cell recordings on HEK-293 and CHO cells, bath solution contained 156 mmol/L NaCl, 5 mmol/L $CaCl_2$, 10 mmol/L glucose, and 10 mmol/L HEPES (pH 7.2) (buffer A). Pipette solution was composed of 156 mmol/L CsCl, 1 mmol/L $MgCl_2$, 10 mmol/L EGTA, and 10 mmol/L HEPES (pH 7.4) (buffer B). Free Ca^{2+} in the pipette solution was 0.02 and 7.4 μmol/L by addition of $CaCl_2$. Ca^{2+} concentrations were measured with the Ca^{2+}-sensitive dye Fluo4FF (Molecular Probes). Holding potential was -60 mV; current traces were elicited by voltage ramps for 250 ms from -120 to $+100$ mV. In the case of single-channel recordings on CHO cells, bath solution contained 140 mmol/L NaCl, 4.8 mmol/L KCl, 1.2 mmol/L $MgCl_2$, 10 mmol/L glucose, and 10 mmol/L HEPES (pH 7.4). Pipette solution contained 145 mmol/L NaCl, 1 mmol/L $CaCl_2$, 1.2 mmol/L $MgCl_2$, 10 mmol/L glucose, and 10 mmol/L HEPES (pH 7.4) (buffer C). For activation of TRPM4 channels, patches were superfused with buffer C (pH 7.2).[15] Recordings were carried out at room temperature (22° to 25°C).

Immunoprecipitation and Western Blot

According to manufacturer instructions, 1.5E6 HEK293 cells per sample were transiently transfected by Lipofectamine 2000 (Invitrogen Inc), with plasmids encoding for Myc-tagged wild-type TRPM4 or mutant TRPM4 channels with or without Ubc9, respectively. Cells were harvested after 24 hours by trypsination and lysed by addition of RIPA-buffer (Sigma Aldrich, Germany). Protein samples were collected by centrifugation and protein amount was measured with Pierce BCA Protein Assay Kit (Thermo Scientific) according to manufacturer instructions. Sheep anti-rabbit IgG Dyna Beads (Invitrogen Inc) were washed 3 times with 0.2% PBS-Tween and afterward incubated with 0.5% BSA (Sigma Aldrich) to prevent unspecific binding of TRPM4 channel. Finally, beads were coated with anti–SUMO-1 antibody (Sigma-Aldrich) at a concentration of 1.7 mg/mL according to manufacturer instructions. To immunoprecipitate SUMOylated proteins, protein samples were incubated with anti–SUMO-1 antibody-coated beads for at least 6 hours at 4°C on a rotating wheel at 12 rpm. After washing of beads 5 times with washing buffer (Thermo Scientific), bound proteins were eluted by 0.1 mol/L Na-citrate buffer (pH 2.5), and solution was afterward neutralized by addition of 1 mol/L Tris buffer (pH 8.7). Samples were subjected to SDS-PAGE on 4% to 12% Bis-Tris gels (Invitrogen Inc) and were transferred to Nitrocellulose membrane (Whatman Inc). Detection of Myc-tagged proteins was carried out with rabbit anti-Myc antibody (Sigma-Aldrich) at a dilution of 1:500 in 2% milk in PBS followed by incubation with HRP-coupled anti-rabbit IgG (Vector Laboratories) at a dilution of 1:2500 in 2% milk in PBS. GAPDH was detected by mouse anti-GAPDH antibody (Sigma-Aldrich) at a dilution of 1:1000 in 2% milk in PBS, HRP-coupled anti-mouse IgG (Jackson ImmunoResearch) at a dilution of 1:4000 in 2% milk in PBS served as secondary antibody.

Immunohistochemistry

Bovine hearts were dissected immediately after death, and tissue samples were rapidly frozen. Tissue samples and sections of 10 μm were kept at -80°C until use. Serial sections were either stained with Masson trichrome or with an anti-TRPM4 polyclonal antibody. This

Downloaded from http://ahajournals.org by on February 7, 2019

TRPM4 antibody was obtained by injecting rabbits with the C terminal oligopeptide (DKRESDSERLKRTSQKV), as in Launay et al[16] (Eurogentec France SASU, Angers, France). Bovine cardiac sections were fixed in cold acetone (−20°C) for 5 minutes, then left to dry for 15 minutes. After washing for 10 minutes 3 times in 1× PBS at room temperature, cardiac sections were incubated in antibody diluent DAKO REAL (Glostrup, Denmark) for 1 hour at room temperature in a moistened chamber. Anti-TRPM4 antibody was added to DAKO REAL at a dilution of 1:50 for further 4 hours of incubation. Sections were then washed 3 times for 10 minutes in 1× PBS and incubated for 2 hours with chicken anti-rabbit antibody labeled with Alexa 488 (Molecular Probes, Invitrogen, The Netherlands) at a dilution of 1:400 in 1× PBS. After being washed for 10 minutes 3 times in 1× PBS at room temperature, sections were mounted and observed with a BX51 Olympus microscope and a 20× UPlanFl objective or on a Spectral confocal microscope (Leica TCS-SP2) equipped with a 63× oil objective (HLX PL APO). Controls were obtained by omitting either the first or the second antibody.

Statistical Analysis

To test for the presence of statistically significant differences between different sample groups in laboratory assessments, the Student *t* test calculation function of Microsoft Excel 2003 was used. Skewed data and unequal variances between groups were taken into account by applying a heteroscedastic *t* test. Probability values below 0.05 were considered significant.

Results

Study Subjects

A large Lebanese kindred with autosomal dominant transmission of Isolated Cardiac Conduction Block (ICCD) was reported previously.[6] It was founded by a polygamous male who engendered several hundred descendants in 4 generations. Only a subset of these descendants was reported. In this family referred to as L1 (Figure 1), several males and females had a variety of conduction blocks including RBBB, frontal left- or right-axis deviation (LAD or RAD), and AV blocks (Table). Family members with a normal ECG or an isolated and incomplete RBBB (QRS duration <120 ms) were considered normal, whereas those with a complete RBBB, an RAD, an LAD, or an AV block either isolated or in combination were considered affected.[6] A single family member with a complete RBBB was considered as a phenocopy on the grounds that his RBBB had a different pattern from all other affected members and because he was carrying a haplotype different in the mutation interval from all other affected members.[9]

The 2 other pedigrees are French. These 2 families are remarkable for the occurrence of a variety of cardiac conduction blocks segregating in an autosomal dominant type of inheritance (Figure 2A and 2B). Several ECG are presented: F1, III5 with an LAD and complete RBBB (online-only Data Supplement Figure 1), F1, IV3 with an LAD and complete RBBB (online-only Data Supplement Figure 2), and F2, IV1 with RAD and complete RBBB (Figure 2C). In pedigree F1, 5 individuals were implanted with a pacemaker at various ages (Table) and a single individual was implanted in pedigree F2 (Table). In this latter pedigree, a female who had a complete RBBB died while sleeping. The autopsy did not discover any drugs or toxics, and the macroscopic and microscopic examination of her heart was normal although specific examination of conduction bundles were not reported.

Altogether, there were 2 cases of LAD (1, 1, and 0 in families L1, F1, and F2, respectively), 10 cases of complete RBBB (5, 1, and 4), 16 cases of incomplete RBBB (14, 0, and 2), 15 cases of complete RBBB with LAD (12, 2, and 1), 6 cases of complete RBBB with RAD (5, 0, and 1), 7 cases of AVBc (7, 5, and 0), and no cases of isolated RAD. Two features were remarkable in these 3 families. First, no family members had an incomplete or complete left bundle-branch block (LBBB). Second, no other cardiac anomalies were reported by repeated cardiac investigations including echocardiograms, stress test, ambulatory ECG and heart scintigraphy. In summary, these families share an autosomal dominant disease giving any conduction block but LBBB and no other cardiac anomalies.

ICCD Locus Mapping

In 1995, we mapped the causal mutation in the large Lebanese kindred (L1)[6] to 19q13 (OMIM %604559). The same polymorphic markers were used with the 2 midsize French families (F1 and F2). Multipoint linkage analysis gave lod scores of 7.2, 2.3, and 1.0 in these 3 families (total multipoint lod score of 10.5), respectively, with a family-specific haplotype shared by all affected family members (except 1 in the L1 family, as noted above). Together, these data defined new borders to the mutation interval (*CABP3* and D19S601), narrowing this interval to 4 megabases of genome containing about 300 Ensembl-predicted genes (http://www.ensembl.org).

Mutation Identification

After testing 12 genes (see online-only Data Supplement for more information), we found a variant in the *TRPM4* gene sequence in each of the 3 families. In the L1 family, a heterozygous missense variation was found in exon 11 (c.1294 G>R) shifting an Alanine to a Threonine at position 432 (Figure 3A). Two heterozygous missense variants were found, 1 in family F1 in exon 5 (c.490 C>Y, p.Arg164Trp) and 1 in family F2 in exon 17 (c.2531 G>R, p.Gly844Asp) (Figure 3B and 3C, respectively[17]). These heterozygous variants were found in all affected family members of each family but also in several family members with incomplete RBBB or no block consistent with an incomplete penetrance as estimated earlier.[9] The family mutation (p.Gly844Asp) was also found in patient III.7 of F2, who died in her sleep (Figure 2B). None of these variants were found in 300 chromosomes of the same ethnic origin. A 2-point linkage analysis with the mutations gave lod score of 6.5, 1.5, and 0.8 (total 8.79) in family L1, F1, and F2, respectively. Mutations Arg164Trp and Ala432Thr are localized to the cytoplasmic TRPM4 N-terminus in regions unrelated to known functional domains. The third mutation (Gly844Asp) maps to an intracellular sequence connecting the second and third TRPM4 transmembrane segments (Figure 3D). These 3 amino acids are highly conserved across vertebrates, as can be seen in online-only Data Supplement Figures 3, 4, and 5. Among the 8 TRPM members of the human genome, only the Ala432 is conserved in all members (online-only Data Supplement Figures 6 to 8). By contrast, Gly844 is included in a peptide segment specific to TRMP4 (online-only Data Supplement Figure 8). Altogether, these data strongly suggested that these

Downloaded from http://ahajournals.org by on February 7, 2019

Table. Clinical Characteristics of Mutation Carriers

Family	Sex	Location	Mutation	Year of Birth	Conduction Block	PM (Age)
L1	Female	II.8	Ala432Thr	1925	RBBBc, LAD	
L1	Female	III.2	Ala432Thr	1920	RBBBc, LAD	
L1	Male	III.5	Ala432Thr	1931	RBBBc	
L1	Female	III.9	Ala432Thr	1925	No block	
L1	Female	III.10	Ala432Thr	1927	No block	
L1	Male	III.13	Ala432Thr	1940	No block	
L1	Male	III.14	Ala432Thr	1941	RBBBi	
L1	Male	III.15	Ala432Thr	1950	RBBBc, LAD	
L1	Female	III.19	Ala432Thr	1969	No block	
L1	Male	IV.1	Ala432Thr	1937	RBBBc, RAD	
L1	Male	IV.3	Ala432Thr	1944	RBBBc, LAD	
L1	Male	IV.5	Ala432Thr	1945	RBBBc, RAD	
L1	Female	IV.10	Ala432Thr	1949	RBBBc, LAD	
L1	Male	IV.13	Ala432Thr	1953	RBBBc, LAD	
L1	Male	IV.15	Ala432Thr	1955	RBBBc	
L1	Male	IV.17	Ala432Thr	1965	No block	
L1	Female	IV.18	Ala432Thr	1972	RBBBc, LAD	
L1	Female	IV.20	Ala432Thr	1976	RBBBc, RAD	
L1	Male	IV.21	Ala432Thr	1978	RBBBc	
L1	Female	IV.22	Ala432Thr	1967	RBBBc, RAD	
L1	Female	IV.28	Ala432Thr	1949	No block	
L1	Female	IV.29	Ala432Thr	1968	No block	
L1	Female	IV.30	Ala432Thr	1966	No block	
L1	Male	IV.33	Ala432Thr	1973	No block	
L1	Male	V.1	Ala432Thr	1970	RBBBc, LAD	
L1	Male	V.2	Ala432Thr	1977	No block	
L1	Male	V.6	Ala432Thr	1976	RBBBc, LAD	
L1	Female	V.7	Ala432Thr	1975	No block	
L1	Female	V.8	Ala432Thr	1976	RBBBi	
L1	Male	V.9	Ala432Thr	1977	RBBBc, LAD	
L1	Female	V.12	Ala432Thr	1974	RBBBc, RAD	
L1	Female	V.25	Ala432Thr	1973	RBBBc, LAD	
L1	Female	V.26	Ala432Thr	1977	No block	
L1	Male	V.27	Ala432Thr	1982	No block	
L1	Male	V.28	Ala432Thr	1985	RBBBc	
F1	Female	I.2	Arg164Trp	1915	LAD	
F1	Female	II.3	Arg164Trp	1935	AVBc	PM (?)
F1	Male	II.4	Arg164Trp	1938	AVBc	PM (45)
F1	Female	III.1	Arg164Trp	1960	AVBc	PM (16)
F1	Female	III.2	Arg164Trp	1965	No block	
F1	Female	III.5	Arg164Trp	1963	RBBBc, LAD	
F1	Female	III.7	Arg164Trp	1966	AVBc	PM (11)
F1	Male	III.8	Arg164Trp	1971	RBBBc	
F1	Female	IV.1	Arg164Trp	1983	No block	
F1	Female	IV.2	Arg164Trp	1990	No block	
F1	Female	IV.3	Arg164Trp	1987	RBBBc, LAD	
F1	Female	IV.4	Arg164Trp	1990	AVBc	PM (<1)
F2	Male	II.1	Gly844Asp	1932	RBBBc, LAD	PM (64)

(*Continued*)

Downloaded from http://ahajournals.org by on February 7, 2019

Table. Continued

Family	Sex	Location	Mutation	Year of Birth	Conduction Block	PM (Age)
F2	Female	II.4	Gly844Asp	1937?	RBBBi	
F2	Male	II.5	Gly844Asp	1941	RBBBc	
F2	Male	III.2	Gly844Asp	1956	RBBBc	
F2	Female	III.4	Gly844Asp	1963	RBBBc	
F2	Female	III.5	Gly844Asp	1966	RBBBi	
F2	Female	III.7	Gly844Asp	1964	RBBBc	SD
F2	Female	III.9	Gly844Asp	1965	No block	
F2	Male	IV.1	Gly844Asp	1984	RBBBc, RAD	
F2	Male	IV.6	Gly844Asp	1999	No block	

AVBc indicates complete atrioventricular block; LAD, left QRS axis deviation; PM (age), pacemaker (year of first implantation); RAD, right QRS axis deviation; RBBBc, complete right bundle-branch block; RBBBi, incomplete right bundle-branch block; and SD.

TRPM4 variants are actually causative mutations in these 3 ICCD families. Based on this assumption, the penetrance can be evaluated at 75% for males (21 carriers with conduction block of 28 carriers) and 54% for females (20/37). These penetrance values are consistent with previous estimations.[9]

Electrophysiological Characterization of TRPM4 Mutants

To understand the functional significance of the ICCD mutations, we studied their mutational effect on human TRPM4 channel expressed in human embryonic kidney cells (HEK-293). As a measure of TRPM4 channel activity, we first analyzed TRPM4-mediated current density. We observed dramatically elevated current amplitudes for TRPM4 mutants ($TRPM4^{Arg164Trp}$, 91.1±20.9 pA/pF, SEM, n=5; $TRPM4^{Ala432Thr}$, 86.3±21.0 pA/pF, SEM, n=5; and $TRPM4^{Gly844Asp}$, 152.6±15.7 pA/pF, SEM, n=5) in comparison to wild-type (18.8±3.7 pA/pF, SEM, n=10) (Figure 4A and 4B). Essentially the same increase in current amplitude was seen after transfection of HEK-293 cells with a 1:1 mixture of wild-type and mutant TRPM4 cDNAs, (TRPM4/$TRPM4^{Arg164Trp}$, 89.0±31.9 pA/pF, SEM, n=6; TRPM4/$TRPM4^{Ala432Thr}$, 92.0±20.3 pA/pF; SEM, n=5, and TRPM4/$TRPM4^{Gly844Asp}$, 119.0±26.5 pA/pF, SEM, n=10) (Figure 4B) consistent with the dominant inheritance of ICCD phenotype. In an attempt to identify the nature of the observed increase in current density and as intracellular Ca^{2+} is a known and important regulator of TRPM4 channel activity,[18] we analyzed Ca^{2+} dependence of wild-type and mutant TRPM4 channels. Interestingly, we found no increase in Ca^{2+} affinity of mutant channels in relation to wild-type channel (Figure 4C and 4D). The results showed unchanged K_D values or even a slightly decreased Ca^{2+} affinity for $TRPM4^{Gly844Asp}$ channels. Taken together, these results indicate that a potential increase in Ca^{2+} sensitivity for mutant TRPM4 channels is not the reason for the observed increase in current density. Therefore, we measured current properties in response to a variety of stimuli known to influence TRPM4 channel gating.[19–21] The results showed that wild-type and mutant TRPM4 channels responded in an essentially identical manner to changes in membrane voltage[19] (Figure 4E), phosphatidylinositol-4,5-bisphosphate,[21] (Figure 4F) and an ATP analogon, AMP-PNP[20] (Figure 4G and 4H).

Macroscopic current amplitude (I) is the product of 3 parameters: single-channel conductance (γ), open probability (*Po*), and number of channels (*N*) expressed at the cell surface. Parameters γ and *Po*, biophysical parameters intrinsic to the channel, were not significantly different between wild-type and mutant TRPM4 channels (Figure 5A through 5C). We therefore hypothesized that an increase in the number of channels at the cell surface explained the increase in I. To evaluate parameter *N*, we used FLAG-tagged channels, having similar current densities as

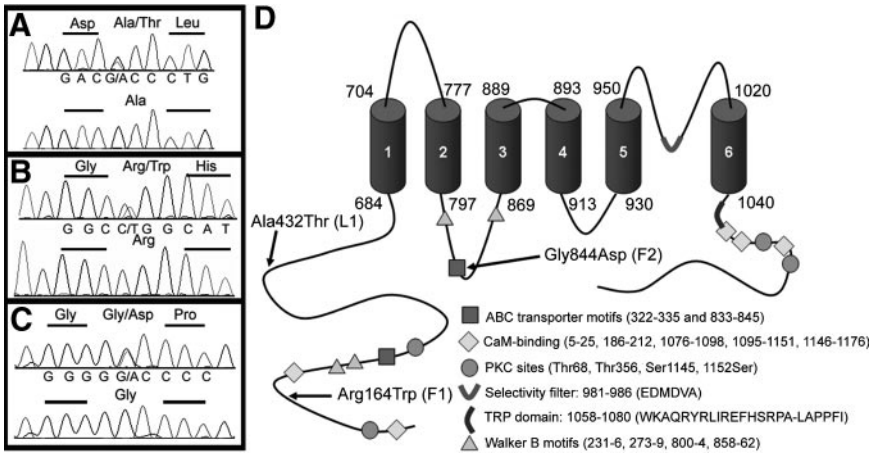

Figure 3. Electrophoregram of heterozygous mutations and schematic representation of the TRPM4 protein. A, p.Ala432Thr mutation of the L1 family. B, p.Arg164Trp mutation of the F1 family. C, p.Gly844Asp mutation of the F2 family. D, predicted topology and functional sites of the TRPM4 protein. The intermediate region contains 6 transmembrane segments.[1–6] The pore region is an extracellular segment located between transmembrane segments 5 and 6. The intracellular segments including the N- and C-terminal regions contain several functional sites. Adapted from Vennekens and Nilius.[17]

Downloaded from http://ahajournals.org by on February 7, 2019

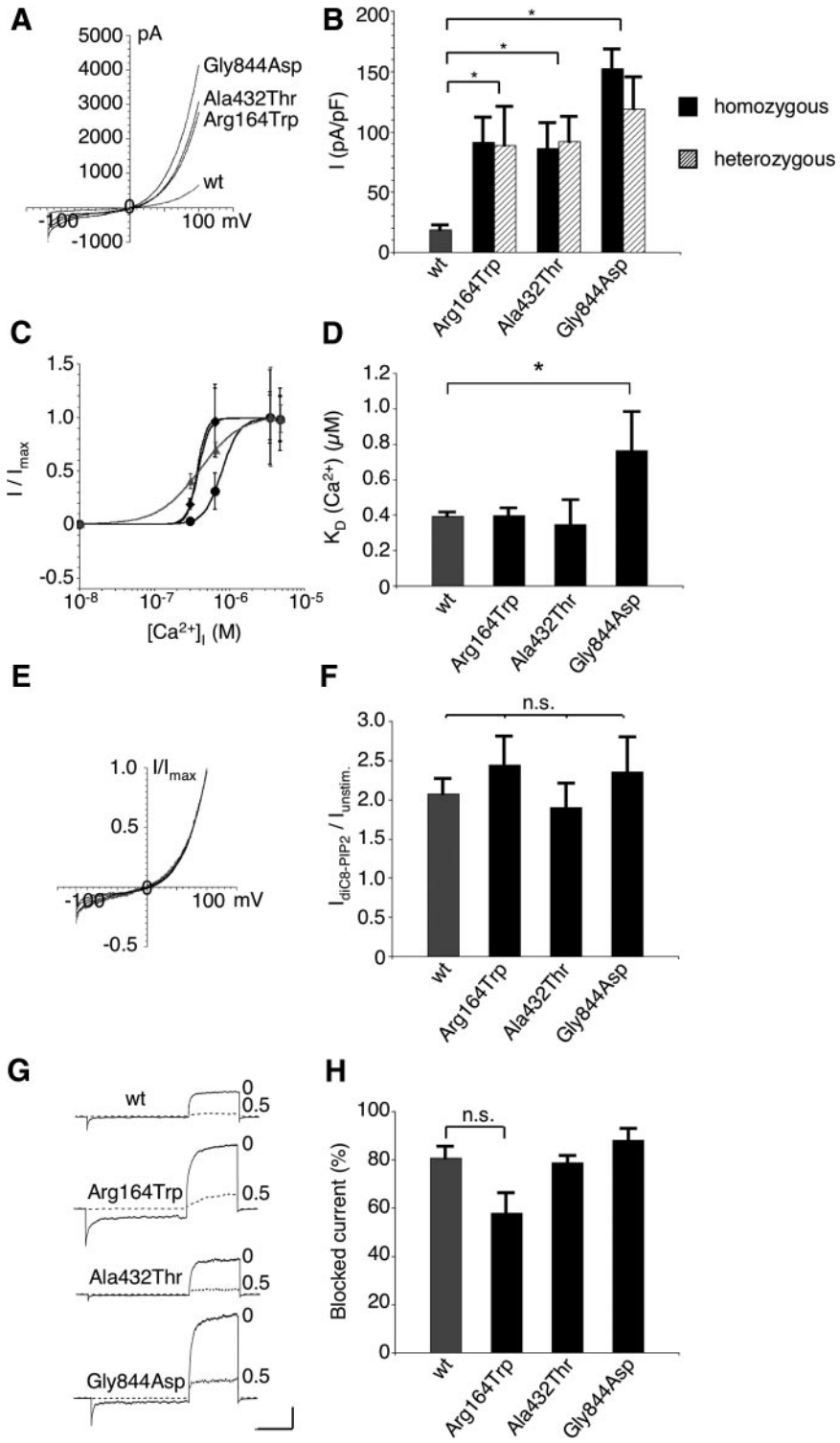

Figure 4. Expression of mutant TRPM4 channels increases TRPM4-mediated current density. A, Current traces of $TRPM4^{wt}$, $TRPM4^{Arg164Trp}$, $TRPM4^{Ala432Thr}$, and $TRPM4^{Gly844Asp}$ channels transiently expressed in HEK293 cells. Traces were extracted from 250-ms voltage-ramps from −120 to 100 mV. Holding potential was −60 mV. B, Current densities of TRPM4 and mutant TRPM4 channels expressed alone or in a 1:1 ratio with wild-type TRPM4 channel measured at 80 mV from voltage-ramps, as shown in A. Values are given as mean±SEM (n [wt]=9, n [mutants]=5, n [wt/mutants]=7 to 13; $P<0.05$). C, HEK293 cells expressing wild-type and mutant TRPM4 channels were recorded in the whole-cell patch-clamp configuration with different concentrations of free Ca^{2+} in the pipette solution. Ca^{2+} dependence of TRPM4-mediated currents was analyzed with voltage-ramp protocols, as described in A. Figure displays normalized current densities at 80 mV (n=10 to 16). $TRPM4^{wt}$: ▲; $TRPM4^{Arg164Trp}$: ■; $TRPM4^{Ala432Thr}$: ♦; $TRPM4^{Gly844Asp}$: ●. D, Bar graphs show K_D (Ca^{2+}, in μM) calculated from traces shown in C. Values are given as mean±SD (n=10 to 16, $^*P<0.05$). E, Traces given in A were normalized to maximal current amplitude to display current-voltage relationship of $TRPM4^{wt}$ and mutant TRPM4 channels. F, Currents conducted by TRPM4 or mutant TRPM4 channels were recorded in the inside-out patch-clamp configuration. From a holding potential of 0 mV, membranes were first hyperpolarized to −100 mV for 500 ms followed by a 250-ms depolarization to 100 mV. TRPM4-mediated currents were recorded with and without exposure of patches to 10 μmol/L diC8-PtdIns(4,5)P_2. Bar graphs show fold change of current amplitude after application of 10 μmol/L diC8-PtdIns(4,5)P_2 (mean±SEM, n=3 to 7). NS indicates not significant. G, Inside-out patch-clamp recordings of wild-type and mutant TRPM4 channels were performed as described in F. Currents were recorded before (0) and after (0.5) the application of 0.5 mmol/L AMP-PNP. Scale bars: 200 ms, 0.5 nA. H, Bar graphs show current blockade in percent after application of 0.5 mmol/L AMP-PNP (mean±SEM, n=3 to 5).

Downloaded from http://ahajournals.org by on February 7, 2019

untagged controls,[5] to analyze TRPM4 protein concentration in transfected cells. Quantitative analysis of immunostained cells (ImageJ, http://rsbweb.nih.gov/if/) expressing FLAG-tagged wild-type or mutant TRPM4 showed a significantly increased immunofluorescence intensity of mutant TRPM4 channels compared with wild-type control (Figure 5D and 5E). In conclusion, these data supported our hypothesis that the ICCD mutations elevated the number of TRPM4 channels (*N*) expressed at the cell surface.

TRPM4 Endocytosis Disturbance

We considered as a likely explanation for increased TRPM4-channel density a default in retrograde TRPM4 trafficking involving dynein-based endocytosis. Accordingly, we co-transfected HEK-293 cells with TRPM4 and dynamitin which disrupts the dynein motor system and interferes with ion channel endocytosis.[12,22] The results showed that coexpression with dynamitin resulted in significantly increased wild-type TRPM4 current density (39.3±7.9 pA/pF, SEM, n=9),

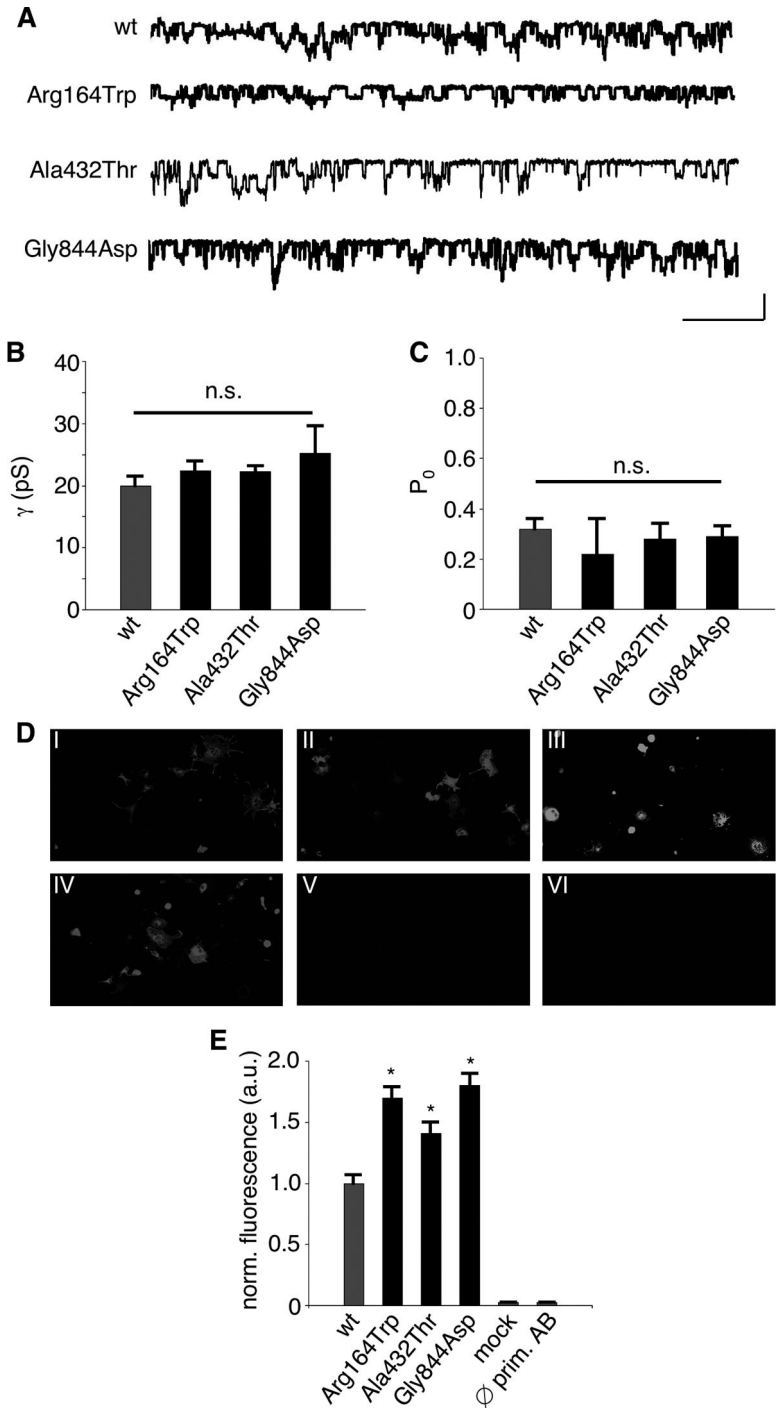

Figure 5. Analysis of TRPM4 density at the cell surface. A, Single-channel currents of $TRPM4^{wt}$, $TRPM4^{Arg164Trp}$, $TRPM4^{Ala432Thr}$, and $TRPM4^{Gly844Asp}$ channels were recorded in the inside-out patch-clamp configuration at −100 mV. Scale bars: 1 second, 5 pA. B, Single channel conductances (γ) of wild-type and mutant TRPM4 channels (mean±SEM; n=9 to 17; NS, not significant). C, Open probability (P_O) of wild-type and mutant TRPM4 channels at −100 mV (mean±SEM; n=9 to 17; NS). D, COS7-cells were transiently transfected with FLAG-$TRPM4^{wt}$ (I), FLAG-$TRPM4^{Arg164Trp}$ (II), FLAG-$TRPM4^{Ala432Thr}$ (III), and FLAG-$TRPM4^{Gly844Asp}$ (IV) and stained with anti-FLAG antibody. Mock-transfected COS7-cells (V) stained with primary and secondary antibody or FLAG-$TRPM4^{wt}$ transfected COS7-cells (VI) stained with secondary antibody only served as controls. E, Immunofluorescence intensity in arbitrary units (a.u.) of FLAG-$TRPM4^{Arg164Trp}$, FLAG-$TRPM4^{Ala432Thr}$, FLAG-$TRPM4^{Gly844Asp}$, mock-transfected COS7-cells, or FLAG-$TRPM4^{wt}$ COS7 cells stained with secondary antibody only (ø prim, AB) normalized to that of FLAG-$TRPM4^{wt}$-expressing cells (mean±SEM, n=60; $P<0.01$).

Downloaded from http://ahajournals.org by on February 7, 2019

whereas current density of mutant TRPM4 channels was dynamitin-insensitive ($TRPM4^{Arg164Trp}$, 120.0±24.9 pA/pF, n=5; $TRPM4^{Ala432Thr}$, 83.6±23.0 pA/pF, n=5; and $TRPM4^{Gly844Asp}$, 153.9±11.2 pA/pF, n=6) (Figure 6A). These data are consistent with a negative impact of ICCD mutations on endocytotic TRPM4 trafficking.

TRPM4 SUMOylation/deSUMOylation Impairment

The SUMO system contributes to the regulation of numerous biological pathways. Because SUMOylation is implied in the regulation of TRPM4 channel activity,[5] we tested whether any of the 3 TRPM4 mutations could alter SUMOylation-dependent channel activity. Wild-type and mutant TRPM4 cDNAs were coexpressed with the SUMO conjugating enzyme Ubc9. SUMOylation is a 3-step process, and Ubc9 is the unique enzyme of the second step, responsible for conjugation of SUMO to its target protein in eukaryotic cells.[23] Coexpression of TRPM4s and Ubc9 produced a significant increase in current density mediated by wild-type TRPM4, $TRPM4^{Ala432Thr}$, and $TRPM4^{Gly844Asp}$ channels, respectively, but we observed no change in current density mediated by $TRPM4^{Arg164Trp}$ channel (Figure 6B). Because deconjugation of SUMO is carried out by SENP1 (Sentrin-specific peptidase 1), we tested whether deconjugation of

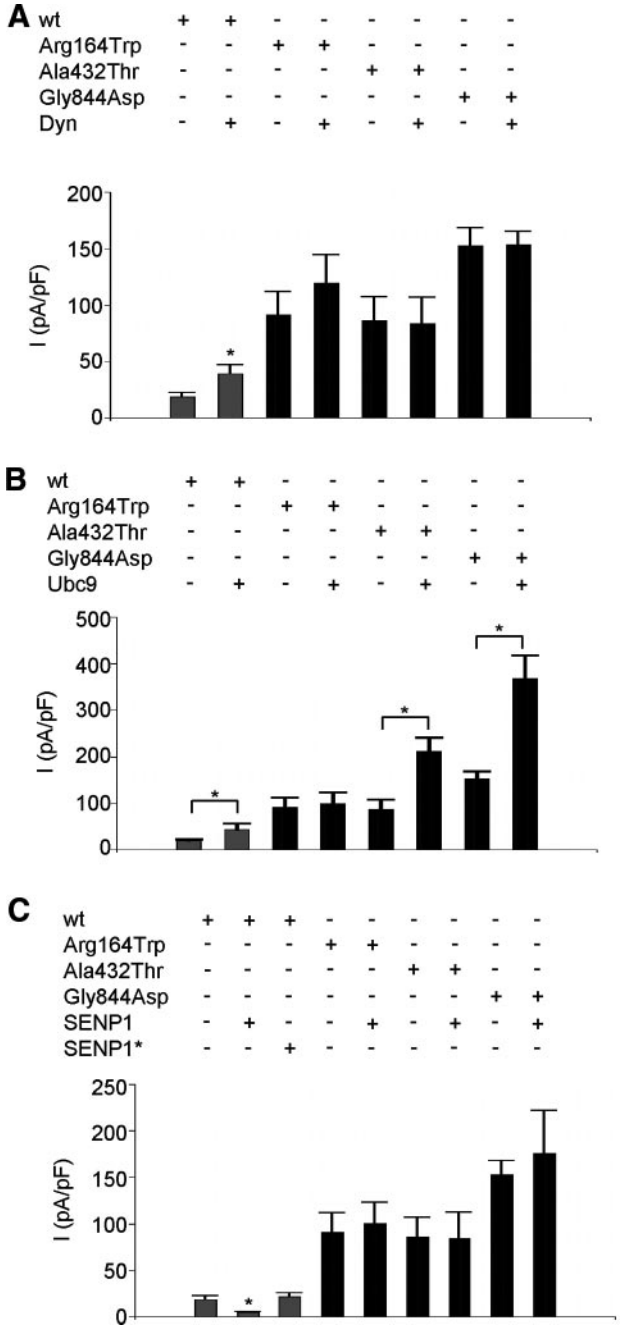

Figure 6. Regulation of TRPM4 channel activity by posttranslational modification. A, Wild-type and mutant TRPM4 channels expressed in HEK293 cells together with or without dynamitin (Dyn), as indicated on top of bar graph. Current densities (pA/pF) were determined at +80 mV, as described in Figure 4A (mean±SEM, n=9 to 10). B, Current density in HEK293 cells of wild-type and mutant TRPM4 channels with or without Ubc9—the conjugating enzyme of SUMO. Experimental conditions as in 6A. C, Same experiment as in (A), but wild-type and mutant TRPM4 channel were coexpressed either with SENP1 or an inactive SENP1 mutant (SENP1*: SENP1–C603S), as indicated on top of the bar graph (mean±SEM; n=6 to 13).

SUMO (deSUMOylation) would change current density of mutant TRPM4 channels. Therefore, we coexpressed SENP1 with TRPM4s. We observed a decrease of wild-type TRPM4 current density to background level (4.5±1.0 pA/pF, SEM for TRPM4+SENP1, n=8 versus 3.5±0.4 pA/pF, SEM for background current, n=7), whereas mutant TRPM4 channel–mediated current densities remained unchanged. Coexpression of wild-type TRPM4 with an inactive SENP1 protease mutant (SENP1-C603S) did not change TRPM4-mediated current density (Figure 6C).[24]

To test whether the increase in current density is associated with increased levels of SUMOylation of TRPM4 channels on coexpression with Ubc9, we isolated protein lysates of HEK293 cells transiently transfected with Myc-tagged TRPM4 channels with or without Ubc9 and immunoprecipitated SUMOylated proteins with anti–SUMO-1 antibody. Immunoprecipitates were subjected to SDS-PAGE and Western blot with anti-Myc antibody to detect SUMOylated TRPM4 channels (Figure 7A). For comparison with total TRPM4 protein amount, we directly analyzed protein lysates in Western blot with anti-Myc antibody, whereas staining with a GAPDH antibody served as a measure for equal loading (Figure 7B). We detected SUMOylated wild-type and mutant TRPM4 channels with no increase of SUMOylated TRPM4 channels on coexpression with Ubc9. On Western blot, the total amount of wild-type TRPM4 is not modified by Ubc9 cotransfection, whereas TRPM4 mutants are slightly decreased on cotransfection with Ubc9.

Immunohistochemistry

To test whether TRPM4 was expressed in specific regions of the heart, we used anti-TRPM4 sera on sections of bovine hearts. A weak signal was obtained on ventricular sections (Figure 8A and B). The level of fluorescence was slightly higher in common atrial cardiomyocytes than in ventricular cardiomyocytes, as can be seen on pieces of right atrium and right ventricle frozen side by side (Figure 8C). By contrast, on tissue blocks of the interventricular septum, we could detect highly labeled cells that were located under the endocardium (Figure 8D and 8E). The morphology of these cells, their organization in small groups surrounded by a thin layer of connective tissue, and their localization identified them as Purkinje fibers.[25,26] Subendocardial bundles of Purkinje fibers branch away to form penetrating bundles directed toward the subepicardial layer to spread the depolarization wave to common cardiomyocytes.[25] Accordingly, we observed bundles of TRPM4 positive cells within the ventricular wall. TRPM4 has a diffuse pattern of distribution in bovine Purkinje fibers. On occasion, it was possible to detect a striated pattern reminiscent of myofibril striation. Purkinje fibers have few myofibrils, and it is possible that TRPM4 channels map to a specific structure of these myofibrils (Figure 8F).

Discussion

The present study, along with the one of Kruse,[5] identifies an essential role for calcium-activated nonselective cation channel (CAN-channel) activity in the cardiac conduction system and establishes ICCD and PFHB1 (Progressive Familial Heart Block type 1) as a CAN channelopathy caused by gain-of-TRPM4 channel function.

Channels are constantly subjected to trafficking toward the plasma membrane and endocytosis so that cell-surface expression at steady state represents a balance between the 2

Downloaded from http://ahajournals.org by on February 7, 2019

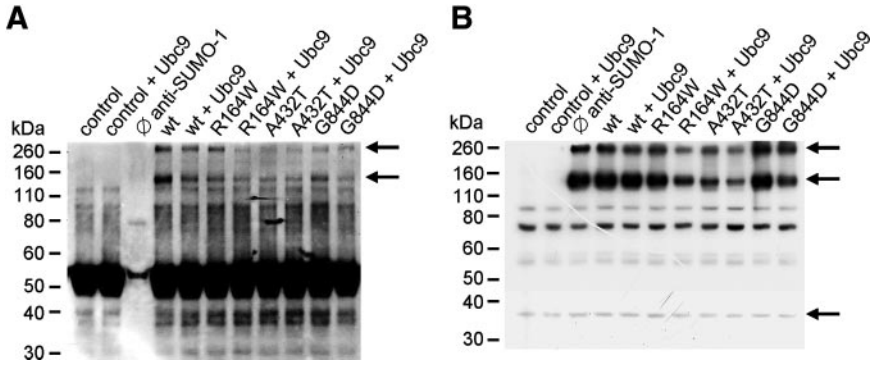

Figure 7. SUMOylation of TRPM4 channels on coexpression with Ubc9. A, HEK293 cells were transiently transfected with plasmids encoding for Myc-tagged wild-type and mutant TRPM4 channels with or without Ubc9, as indicated on top of the figure. Protein lysates were harvested as described in Material and Methods and incubated with anti–SUMO-1 antibody-coated beads. Immunoprecipitated proteins were eluted from beads and subjected to SDS-PAGE and Western blot with anti-Myc antibody. Control indicates lysates from HEK293 cells being nontransfected; control+Ubc9 indicates transfection with a plasmid encoding for Ubc9 only; anti–SUMO-1 indicates lysate from HEK293 cells transfected with a plasmid encoding for Myc-tagged TRPM4 channel, which was treated with beads that had not been coated with anti–SUMO-1 antibody. Arrows indicate expected bands for nonglycosylated (upper arrow) and glycosylated (upper arrow) TRPM4 channels. B, Same as in A, but lysates were not treated with antibody-coated beads. Whole-cell protein lysates were subjected to SDS-PAGE and Western blot with anti-Myc antibody and anti-GAPDH antibody to compare for equal loading. Arrows indicate expected bands for nonglycosylated (middle arrow) and glycosylated (upper arrow) TRPM4 channels; lower arrow indicates expected band for GAPDH.

movements. A recent awareness that trafficking might be impeded by channel mutations has revealed that it is actually the case in numerous mutations in long QT[27,28] and sinus node[29,30] syndromes. The consequence of a single mutation is usually diverse, with impact on biophysical properties, sensibility to factors influencing gating properties, and trafficking. The combination of these alterations that individually may have opposite consequences results in a gain or—more often—a loss of function. Because TRPM4 mutations in conduction block were associated with a gain of function, we evaluated endocytosis, speculating that a decrease of trafficking away from the plasma membrane might contribute to this increase in current density. Cytoplasmic dynein binds to its cargo by a dynactin complex, but overexpression of dyna-

Downloaded from http://ahajournals.org by on February 7, 2019

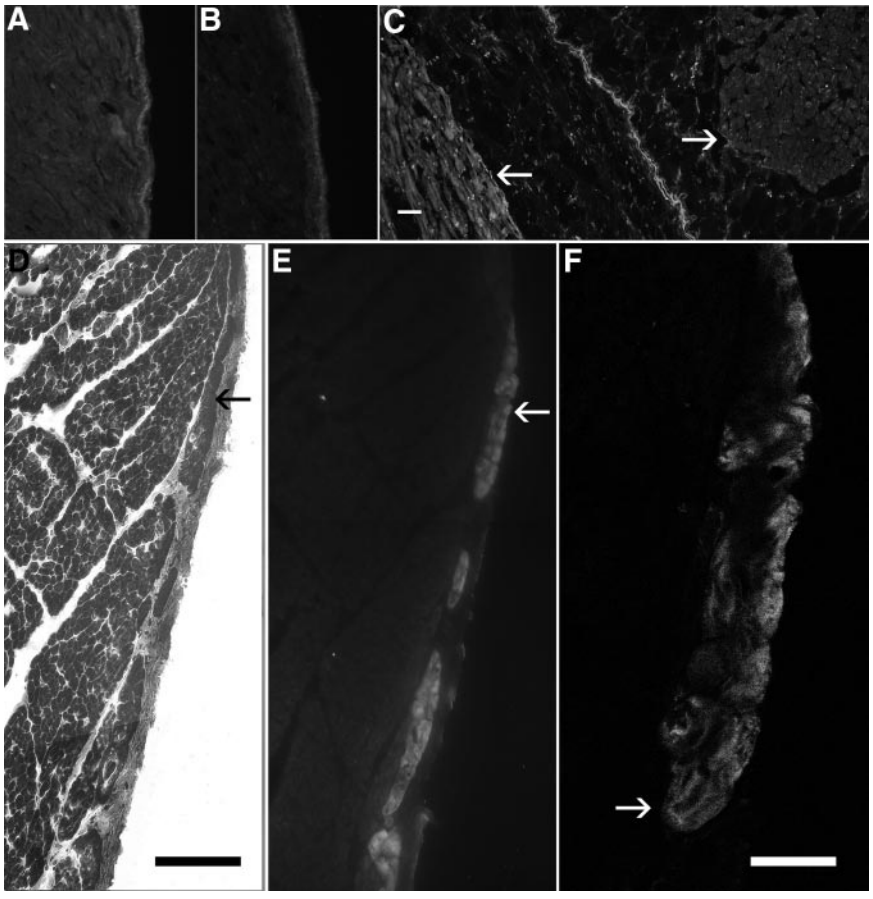

Figure 8. Immunohistochemistry of bovine hearts labeled with anti-TRPM4 antibody. Serial sections of bovine ventricle were either labeled with rabbit anti-TRPM4 antibody and chicken anti-rabbit antibody labeled with Alexa 488 (A) or with rabbit preimmune serum and the same secondary antibody as control (B). Both sections were exposed with the same parameters. Whereas the autofluorescence of the endocardium is identical in both images, the level of fluorescence is slightly higher in the anti-TRPM4 section than in the control. C, Samples of right atrium and right ventricle were positioned side by side and frozen. Atrial cardiomyocytes (left-hand side) are more highly labeled than ventricular cardiomyocytes (right-hand side). Cardiomyocytes (white arrows) are separated by atrial and ventricular endocardium. Serial sections of the interventricular septum were stained with Masson trichrome (D) or labeled with anti-TRPM4 antibody (E). TRPM4 revealed bundles of highly labeled cells that are located under the endocardium (F). Under a confocal microscope, a magnification of the bundle pointed by the white arrow in D and E shows a cellular distribution of TRPM4, which appears unstructured except in some areas where a striation pattern is visible (see white arrow). Scale bars: 140 μm in A to E and 40 μm in F.

mitin—one of the subunits of dynactin—disrupts the dynactin complex and dissociates dynein from its cargo, stopping all dynein-dependent cellular events.[12,22] None of the 3 TRPM4 mutant channels had an increase in current density after overexpression of dynamitin, suggesting that removal of TRPM4 channels was impaired as a consequence of mutations.

SUMO conjugation (SUMOylation) is a reversible post-translational protein modification recognized as an important regulatory method used by the cell to modulate the activity, stability, or localization of intracellular proteins.[23] Cotransfection experiments of TRPM4 mutants with Ubc9 showed that Ala432Thr and Gly844Asp had—as wild-type TRPM4—an increased of current density, whereas Arg164Trp had no change. These data demonstrate that the stimulation of wild-type TRPM4 SUMOylation increased current density. Furthermore, it showed that the stimulation of Ala432Thr and Gly844Asp but not Arg164Trp SUMOylation was possible. Coexpression of TRPM4 mutants with SEN1P—an enzyme that stimulates deconjugation of SUMO—decreased wild-type TRPM4 current density to background level. By contrast, all TRPM4 mutants were insensitive to SENP1, indicating that deSUMOylation of mutant TRPM4 channels is impaired or has no consequence (because dynein-based removal is already inactivated). Interestingly, we found no alteration in the amount of SUMOylated TRPM4 channels on coexpression of Ubc9, although we detected an increase in current density for most TRPM4 channels if coexpressed with Ubc9. Taken together, these data demonstrate that TRPM4 is at least partly regulated by SUMO. SUMOylation might be an important signal in the control of TRPM4 channel trafficking to the plasma membrane and/or in directing endocytosed TRPM4 channels to degradation or recycling to the membrane. It can also be concluded that the 3 reported mutations hitting diverse parts of the TRPM4 channel result in a variety of elementary dysfunctions that finally concurred to an increased current density. For instance, Ubc9 cotransfection increased current density of Ala432Thr and Gly844Asp but did not change Arg164Trp current density, and the Western blot showed normal (Arg164Trp and Gly844Asp) or decreased (Ala432Thr) total amount of TRPM4. Further studies are warranted to decipher all the elementary cellular mechanisms that modulate channel activity. We could not draw any definite correlation between any of these elementary cellular dysfunctions and the apparent more severe phenotype of family F1, which has the highest percentage of complete AV block including the only pediatric one.

The fact that no LBBB was observed in these families is not fortuitous. It might be related to the observation that the left branch of the His bundle does not exist. The His bundle gives rise first to numerous and fine bundles directed toward the posterior wall of the left ventricle. A few millimeters further down, the bundle destinated to the left ventricle anterior wall originates, leaving the right bundle-branch.[31]

Taken together, these data demonstrate a causative role of TRPM4 mutations in ICCD. The common electrophysiological consequence of these diverse mutations is an increase in current density secondary to modifications in the regulation of channel density. It is likely that elevated density of TRPM4 channels at the cell surface increases membrane leak conductance, disabling action potential propagation down the Purkinje fibers. These data warrant further studies to improve the understanding of the interplay between TRPM4 channels and other cardiac channels.

Downloaded from http://ahajournals.org by on February 7, 2019

Acknowledgments

We thank the participating families. We especially thank Dr Edouard Stephan of Beirut, Lebanon, who identified the Lebanese family and was a strong stimulator for this study until his death in 2005. Dr Bouvagnet thanks Pierre Launay for fruitful discussions. Drs Kruse and Pongs thank G. Sachse for critical discussion and Y. Wu and N. Kursawe for great help and advice in performing coimmunoprecipitation experiments. Yves Tourneur and the Centre Commun de Quantimétrie (Université de Lyon 1, Lyon, France) are warmly thanked for providing access to the confocal microscope and giving expert suggestions.

Sources of Funding

This study was supported by a grant to Dr Bouvagnet (Projet Hospitalier de Recherche Clinique 2003 and 2008, Fondation Renaud Febvre) and by the Deutsche Forschungsgemeinschaft to Dr Pongs (Po 137/37-2 [FOR 604] and Po 137/39-1 [FOR 885]). Dr El Zein was supported by a stipend from Centre National de la Recherche Scientifique of Lebanon.

Disclosures

None.

References

1. Chiu SN, Wang JK, Wu MH, Chang CW, Chen CA, Lin MT, Wu ET, Hua YC, Lue HC. Cardiac conduction disturbance detected in a pediatric population. *J Pediatr*. 2008;152:85–89.
2. Miller WL, Hodge DO, Hammill SC. Association of uncomplicated electrocardiographic conduction blocks with subsequent cardiac morbidity in a community-based population (Olmsted County, Minnesota). *Am J Cardiol*. 2008;101:102–106.
3. Schott JJ, Alshinawi C, Kyndt F, Probst V, Hoorntje TM, Hulsbeek M, Wilde AA, Escande D, Mannens MM, Le Marec H. Cardiac conduction defects associate with mutations in SCN5A. *Nat Genet*. 1999;23:20–21.
4. Schott JJ, Benson DW, Basson CT, Pease W, Silberbach GM, Moak JP, Maron BJ, Seidman CE, Seidman JG. Congenital heart disease caused by mutations in the transcription factor NKX2–5. *Science*. 1998;281:108–111.
5. Kruse M, Schulze-Bahr E, Corfield V, Beckmann A, Stallmeyer B, Kurtbay G, Ohmert I, Brink P, Pongs O. Impaired endocytosis of the ion channel TRPM4 is associated with human progressive familial heart block type I. *J Clin Invest*. 2009;119:2737–2744.
6. de Meeus A, Stephan E, Debrus S, Jean MK, Loiselet J, Weissenbach J, Demaille J, Bouvagnet P. An isolated cardiac conduction disease maps to chromosome 19q. *Circ Res*. 1995;77:735–740.
7. Hoffmann K, Lindner TH. easyLINKAGE-Plus: automated linkage analyses using large-scale SNP data. *Bioinformatics*. 2005;21:3565–3567.
8. Kruglyak L, Lander ES. Faster multipoint linkage analysis using Fourier transforms. *J Comput Biol*. 1998;5:1–7.
9. Stephan E, de Meeus A, Bouvagnet P. Hereditary bundle branch defect: right bundle branch blocks of different causes have different morphologic characteristics. *Am Heart J*. 1997;133:249–256.
10. Fliegert R, Glassmeier G, Schmid F, Cornils K, Genisyuerek S, Harneit A, Schwarz JR, Guse AH. Modulation of Ca2+ entry and plasma membrane potential by human TRPM4b. *FEBS J*. 2007;274:704–713.
11. Ahmad FJ, Echeverri CJ, Vallee RB, Baas PW. Cytoplasmic dynein and dynactin are required for the transport of microtubules into the axon. *J Cell Biol*. 1998;140:391–401.
12. Burkhardt JK, Echeverri CJ, Nilsson T, Vallee RB. Overexpression of the dynamitin (p50) subunit of the dynactin complex disrupts dynein-dependent maintenance of membrane organelle distribution. *J Cell Biol*. 1997;139:469–484.

13. Bailey D, O'Hare P. Herpes simplex virus 1 ICP0 co-localizes with a SUMO-specific protease. *J Gen Virol*. 2002;83:2951–2964.
14. Schmidt D, Muller S. Members of the PIAS family act as SUMO ligases for c-Jun and p53 and repress p53 activity. *Proc Natl Acad Sci U S A*. 2002;99:2872–2877.
15. Demion M, Bois P, Launay P, Guinamard R. TRPM4, a Ca2+-activated nonselective cation channel in mouse sino-atrial node cells. *Cardiovasc Res*. 2007;73:531–538.
16. Launay P, Cheng H, Srivatsan S, Penner R, Fleig A, Kinet JP. TRPM4 regulates calcium oscillations after T cell activation. *Science*. 2004;306: 1374–1377.
17. Vennekens R, Nilius B. Insights into TRPM4 function, regulation and physiological role. *Handb Exp Pharmacol*. 2007:269–285.
18. Launay P, Fleig A, Perraud AL, Scharenberg AM, Penner R, Kinet JP. TRPM4 is a Ca2+-activated nonselective cation channel mediating cell membrane depolarization. *Cell*. 2002;109:397–407.
19. Nilius B, Prenen J, Droogmans G, Voets T, Vennekens R, Freichel M, Wissenbach U, Flockerzi V. Voltage dependence of the Ca2+-activated cation channel TRPM4. *J Biol Chem*. 2003;278:30813–30820.
20. Nilius B, Prenen J, Voets T, Droogmans G. Intracellular nucleotides and polyamines inhibit the Ca2+-activated cation channel TRPM4b. *Pflugers Arch*. 2004;448:70–75.
21. Voets T, Nilius B. Modulation of TRPs by PIPs. *J Physiol*. 2007;582: 939–944.
22. Valetti C, Wetzel DM, Schrader M, Hasbani MJ, Gill SR, Kreis TE, Schroer TA. Role of dynactin in endocytic traffic: effects of dynamitin overexpression and colocalization with CLIP-170. *Mol Biol Cell*. 1999; 10:4107–4120.
23. Ulrich HD. The SUMO system: an overview. *Methods Mol Biol*. 2009; 497:3–16.
24. Xu Z, Chau SF, Lam KH, Chan HY, Ng TB, Au SW. Crystal structure of the SENP1 mutant C603S-SUMO complex reveals the hydrolytic mechanism of SUMO-specific protease. *Biochem J*. 2006;398:345–352.
25. Oosthoek PW, Viragh S, Lamers WH, Moorman AF. Immunohistochemical delineation of the conduction system, II: the atrioventricular node and Purkinje fibers. *Circ Res*. 1993;73:482–491.
26. Virtanen I, Narvanen O, Thornell LE. Monoclonal antibody to desmin purified from cow Purkinje fibers reveals a cell-type specific determinant. *FEBS Lett*. 1990;267:176–178.
27. Anderson CL, Delisle BP, Anson BD, Kilby JA, Will ML, Tester DJ, Gong QM, Zhou ZF, Ackerman MJ, January CT. Most LQT2 mutations reduce Kv11.1 (hERG) current by a class 2 (trafficking-deficient) mechanism. *Circulation*. 2006;113:365–373.
28. Sato A, Arimura T, Makita N, Ishikawa T, Aizawa Y, Ushinohama H, Kimura A. Novel mechanisms of trafficking defect caused by KCNQ1 mutations found in long QT syndrome. *J Biol Chem*. 2009;284: 35122–35133.
29. Nof E, Luria D, Brass D, Marek D, Lahat H, Reznik-Wolf H, Pras E, Dascal N, Eldar M, Glikson M. Point mutation in the HCN4 cardiac ion channel pore affecting synthesis, trafficking, and functional expression is associated with familial asymptomatic sinus bradycardia. *Circulation*. 2007;116:463–470.
30. Ueda K, Nakamura K, Hayashi T, Inagaki N, Takahashi M, Arimura T, Morita H, Higashiuesato Y, Hirano Y, Yasunami M, Takishita S, Yamashina A, Ohe T, Sunamori M, Hiraoka M, Kimura A. Functional characterization of a trafficking-defective HCN4 mutation, D553N, associated with cardiac arrhythmia. *J Biol Chem*. 2004;279:27194–27198.
31. James TN. Structure and function of the sinus node, AV node and His bundle of the human heart: part I-structure. *Prog Cardiovasc Dis*. 2002;45:235–267.

CLINICAL PERSPECTIVE

Isolated cardiac conduction blocks are not infrequent in the general population, prevalent in about 0.5% of children and being more in the 6th decade and above, according to recent surveys. It is generally perceived that isolated cardiac conduction blocks are benign and eventually transitory in the young and may be an early sign of a cardiac disease in elderly people (ischemia, cardiomyopathy?). We report on families with isolated cardiac conduction blocks that resulted from mutation in the *TRPM4* gene. This gene encodes a newly discovered channel permeable to Na^+ and K^+. Isolated cardiac conduction blocks secondary to TRPM4 mutations are neither a transitory benign disease nor a sentinel of a cardiac disease of broader impact because mutation carriers evolved toward permanent and more severe blocks but did not develop any cardiomyopathy, and prevalence of coronary artery disease was similar to that in the general population. This discovery shed a new light on isolated conduction blocks and raises 2 questions. Because TRPM4 isolated conduction blocks are neither transitory nor benign, carriers should be followed up, but what is the actual prevalence of TRPM4 mutation carriers among isolated cardiac conduction blocks, and how could we recognize them? Thus far, we have only clues to the latter question: Diverse conduction blocks were observed but not left bundle-branch block. Moreover, in a previous report, we showed that mutation carriers with a right bundle-branch block had a large R wave in right precordial leads, whereas a noncarrier family member with a right bundle-branch block had instead a deep S wave in the same leads.

Downloaded from http://ahajournals.org by on February 7, 2019